PCCP

ROYAL SOCIETY OF CHEMISTRY

PAPER

View Article Online
View Journal | View Issue

Cite this: *Phys. Chem. Chem. Phys.*, 2026, **28**, 7183

Sulfonium cation $[SF_3]^+$ complexes with noble gases

Mariusz Michalczyk, *[a] Wiktor Zierkiewicz [a] and Pavel Hobza [b]

Received 1st December 2025,
Accepted 18th February 2026

DOI: 10.1039/d5cp04672f

rsc.li/pccp

Chalconium cations are powerful Lewis acids containing a hypervalent chalcogen atom. They are utilized in the field of organocatalysis and crystal engineering. In the current work, the electrophilic force of these species has been examined. The $[SF_3]^+$ chalconium cation was selected for the current study, and its complexes with noble gas atoms were modeled. In this manner, a set of three $[SF_3(NCCH_3)_2Ng]^+$ and $[SF_3(Ng)_2][SbF_6]$ complexes (Ng = Ar, Kr, Xe) were computed. The Ng atom was substituted in place of the anion (in $[SF_3(NCCH_3)_2Ng]^+$) or neutral ligands (in $[SF_3(Ng)_2][SbF_6]$). The computations were performed using a polarizable continuum model. The obtained tetramers were stable, true minima, characterized by weak interaction energies between −2 and −1 kcal mol^{-1}. When the $[SbF_4]^-$ anion was substituted by a noble gas atom, the interaction energy was significantly weakened compared to the full $[SF_3(NCCH_3)_2][SbF_6]$ system, and its nature changed from electrostatic to dispersive. A comparable scenario was observed when the $NCCH_3$ ligands were replaced with two noble gas atoms.

Introduction

Chalconium cations are chemical entities where the core chalcogen atom, in the +II or +IV oxidation state, is hypervalently bonded to three or five atoms, respectively. In this configuration, the cationic individual exhibits substantial electrophilic capabilities, which increase with the electron-withdrawing character of the substituents. This phenomenon has already been observed and utilized in several research studies on the organocatalytic efficacy of chalconium cations, which can stabilize the intermediate phases in organic transformations.[1–5] It has been shown that within this group, the catalytic potential rises from sulfonium to telluronium cations;[6–8] however, sulfonium salts cannot be avoided as they still display considerable catalytic activity toward several model organic reactions.[9,10] Chalconium cations contribute not only to reactions in organic chemistry but also to crystal engineering as supramolecular linkers influential in directional maintenance of the molecular scaffolds.[11–16] The noncovalent interactions observed in numerous crystal structures and transition states in organic reactions involving chalconium cations are labelled as chalcogen bonds.[14,17,18] Their presence is rationalized in terms of the manifestation of a region with a positive molecular electrostatic potential (MEP) at the chalcogen atom (called the σ-hole),[19–21] which acts as an acidic binding site. Consequently, modulation of the acidic strength of the chalcogen species is essential for establishing stable interactions with approaching ligands, irrespective of their role as a transitional state in various organic reactions or in the construction of a supramolecular framework.

The reactivity of chalconium cations has been reported recently in a couple of works. For example, chalconium units were studied in complexes with the $[\beta\text{-}Mo_8O_{26}]^{4-}$ compound.[11] A series of $[Ch(bPh)R]^+$ cations (Ch = S, Se, Te; R = phenyl, 2,4,6-$(CH_3)_3C_6H_2$, 4-BrC_6H_4, 4-FC_6H_4) established stable structures with beta-octamolybdate ligands according to specific patterns. The primary stabilizing interaction occurred between the σ-holes on the chalcogen atoms and the oxygen atoms, supplemented by secondary electrostatic cation–anion interactions. The alteration of the S atom to Se and Te induced a change in the O···O···Ch angle, from 40–50° for the sulfonium cation to 90° for the telluronium analogue.[11] In another work, the reactivity of silylated chalconium ions *versus* the borate and carborate anions was investigated both experimentally and theoretically.[5] The $[T_3S]^+$ and $[T_3O]^+$ cations (T = Me_3Si) were obtained and characterized throughout this study.[5] It should be noted that the arrangement of oxygen as a center of the chalconium cation shown therein is rather scarce. The effectiveness of cyclic sulfonium, selenonium and telluronium cations as catalytic agents in two model reactions, hydrolysis of methyl chloride and addition of ammonia to acetone, was examined by Novikov and Bolotin.[2] The transition states stabilized *via* chalcogen bonds were quantitatively described by DFT-based theoretical predictions. The interaction energies and charge transfer values of the transition states increased from S to Te cations, indicating greater stability for the heavier chalcogens.[2]

[a] *Faculty of Chemistry, Wrocław University of Science and Technology, Wybrzeże Wyspiańskiego 27, 50-370 Wrocław, Poland.*
E-mail: mariusz.michalczyk@pwr.edu.pl
[b] *Institute of Organic Chemistry and Biochemistry, Academy of Sciences of the Czech Republic, v.v.i., Flemingovo Namesti 542/2, 16000 Prague, Czech Republic*

Contrary to previous studies, in the current manuscript, simpler models were chosen to evaluate the principles of the interaction between the sulfonium cation and neutral ligands. We aimed to test the very limits of the ligand-accepting abilities of the sulfonium cation by using the noble gas (Ng) atoms as models of Lewis bases. Noble gases are famous for their limited reactivity, owing to their full valence electronic configuration. The history of studying noncovalent interactions involving Ng atoms is relatively short. The so-called "aerogen bond", where the noble gas atoms produce σ- or π-holes, has been reported several times starting in 2015.[22–29] Recently, Pino-Rios[30] *et al.* performed calculations of systems where the B–Ng (Ng = Ar, Kr, Xe, Rn) covalent bond was formed in $[BH_4–Ng]^+$ synthons. The noble gas···halonium cation interactions were also documented.[31] We demonstrated that these interactions can be accompanied by slight shifts in the σ-hole location. The set of modeled $[X–Xe\cdots Ng]^+$ (X = Cl, Br, I; Ng = Ar, Kr, Xe) complexes was characterized by a wide span of interaction energies from −1 to −25 kcal mol^{-1}. In the current investigation, again three noble gases, namely Ar, Kr and Xe, were utilized as model nucleophiles. To provide experimental context to our work, as a computational prototype of the sulfonium cation, the $[SF_3(NCCH_3)_2][SbF_6]$ compound[32] found in the Cambridge Structural Database[33] was chosen. The presence of both neutral and anionic ligands attached to the $[SF_3]^+$ cation enabled us to assess the interactions between the cation and noble gases in different geometrical scenarios, in which the Ng atoms could be placed in the position of the nitrogen atoms of the neutral ligands or the fluorine atom of the anion. The strength, nature, and properties of chalcogen bonds were explored using a variety of theoretical approaches. We believe that our fundamental study will deliver essential data about the interactions powered by sulfonium cations with highly nonreactive neutral ligands. In our opinion, assessing such borderline cases of chalconium cation interactions is vital to prompting further studies of these fascinating species.

Computational methods

The calculations for the $[SF_3(NCCH_3)_2][SbF_6]$ model taken from the crystal structure (Cambridge Structural Database,[33] ver. 5.44, reference code AMOLUM[32]) and its complexes with noble gases (argon, krypton, xenon) were performed using the M06-2X method and Def2TZVPP[34–37] basis set (containing Stuttgart–Dresden effective core potentials) by means of the Gaussian 16 (Rev. D.01) set of codes.[38] The SCF energy convergence criterion was set to 10^{-8} Hartree, while the geometric convergence criteria were as follows: Maximum Force: 4.50×10^{-4} a.u., RMS Force: 3.00×10^{-4} a.u., Maximum Displacement: 18.00×10^{-4} a.u., RMS Displacement: 12.00×10^{-4} a.u. DFT calculations were conducted using an ultrafine grid with the following parameters: IRadAn = 5 and IXCGrd = 4. In earlier benchmark analyses, the M06-2X functional showed high performance for the investigation of noncovalent interactions.[39,40] The full optimization of the complexes was conducted using the UFF-PCM solvent model and a Lebedev-Laikov grid[41,42] with dichloromethane as the solvent, as the same entity was used in the experiments. The obtained geometries were reviewed in terms of harmonic frequency analysis of the normal modes, which unveiled no imaginary frequencies, confirming them as real minima. The molecular electrostatic potential (MEP) analysis for the $[SF_3(NCCH_3)_2]^+$ and $[SF_3][SbF_6]$ systems was performed to identify maxima of EP at the 0.001 au isocontour of electron density of the sulfonium cation before attaching the Ng atoms. This examination was made using the Multiwfn software (ver. 3.7).[43,44] Graphical representation of the MEPs was achieved using the VMD program (ver. 1.9.4).[45] Decomposition of the interaction energy into its components was accomplished using the ALMO-EDA (Absolutely Localized Molecular Orbitals – Energy Decomposition Analysis) scheme with SMD solvent simulation[46,47] at the M06-2X/def2tzvpp level of theory by the Q-Chem 6 package using the SG-3 grid suitable for the Minnesota functionals and SCF convergence criterion of 10^{-8} Hartree. The basis set superposition error (BSSE) in the interaction energy calculations was removed *via* the counterpoise procedure.[48] The atomic charges were obtained using the CM5,[49] ADCH,[50] AIM,[51] CHELPG[52] and NBO[53] methods. The QTAIM[54,55] "Atoms in Molecules" analysis was performed employing the AIMAll[56] package in order to establish the bond paths and bond critical points in the investigated complexes.

Results

Modelled crystal structure

The fragment of the solid presented in Fig. 1 was fully optimized using simulations under vacuum as well as immersed in a solvent through the polarizable continuum model. Dichloromethane (DCM) was selected as the solvent due to the fact that this organic molecule was employed in the experimental procedures.[32] Only the structure optimized in solvent was chosen for further studies, as that optimized in the gas phase differed substantially from the experimental one. The selection of this specific crystal fragment was determined by the intention to acquire a compound with ligands amenable to facile substitution by a noble gas atom in subsequent modeling.

A comparison between the selected experimental and theoretical geometric parameters (after optimization in the solvent) is given in Table 1. As one can see from this table, the DFT-predicted geometry is more linear on incorporating ligands on the respective extensions of the F–S bond in the cationic entity;

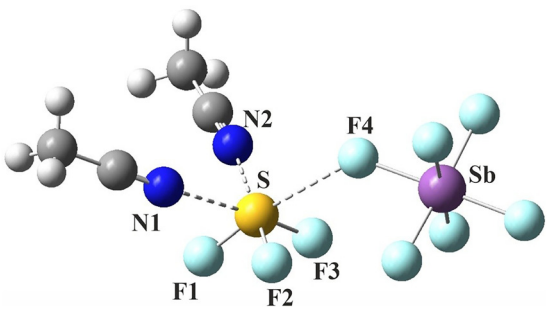

Fig. 1 The $[SF_3(NCCH_3)_2][SbF_6]$ fragment of the X-ray structure (refcode AMOLUM[32]).

Table 1 Selected bond distances (in Å) and bond angles (in °) in the $[SF_3(NCCH_3)_2][SbF_6]$ complex from experiment and calculated at the M06-2X/def2tzvpp level

	Exp.[a]	Theory (DCM as solvent)	Δ[b]
Bond distance			
S–F4	2.621	2.473	−0.148
S–F1	1.509	1.522	0.013
S–F2	1.512	1.526	0.014
S–F3	1.512	1.526	0.014
S–N1	2.462	2.525	0.063
S–N2	2.462	2.520	0.058
Bond angles			
F1–S–F4	172.2	176.0	3.8
F2–S–N2	175.3	176.4	1.1
F3–S–N1	175.3	176.0	0.7

[a] Taken from ref. 32. [b] Differences between theoretical and experimental parameters.

however, all distances except S-F4 are overestimated. It must be added that the RMSD (root mean square deviation) between experiment and theory for a larger set of distances and bond angles is only 0.049 Å and 1.6°, respectively. Thus, the mimicking of the forces met in the crystal structures by DCM was satisfactory. The same results for optimization in the gas phase yielded 0.662 Å and 20.8°, accordingly. Additionally, the superimposition of the structures: crystalline, optimized in the gas phase, and in the implicit solvent medium, is illustrated in Fig. 2. The model of solvent inclusion with DCM was confirmed as far more precise than the default optimization in the gas phase and consequently picked for further modelling within the current work.

For the purpose of later comparison between the optimized crystal structure and models with noble gases, the theoretical characteristics of the studied compound were determined. The investigated complex exhibits interactions between charged and neutral particles; hence, the flow of electron density was important to evaluate. It was measured in terms of the atomic charges, counted by 5 different theoretical protocols. Recently, the ADCH and CM5[57] ones were confirmed as excellent for estimating atomic charges, as they reflected the experimental

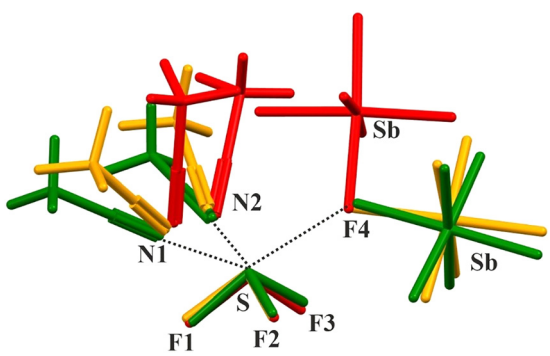

Fig. 2 The superimposition of the structures: nonoptimized crystal (green), optimized in the gas phase (red), and in implicit solvent medium with DCM as the solvent (yellow). The optimization was performed at the M06-2X/def2tzvpp level of theory.

Table 2 Atomic charges on selected atoms of the $[SF_3(NCCH_3)_2][SbF_6]$ complex. Numbering of atoms as in Fig. 1

	CM5	ADCH	AIM	CHELPG	NBO
S	0.718	0.658	2.917	0.908	2.155
F1	−0.040	−0.017	−0.702	−0.059	−0.422
F2	−0.042	−0.009	−0.698	−0.060	−0.424
F3	−0.042	−0.009	−0.698	−0.063	−0.425
F4	−0.305	−0.314	−0.768	−0.481	−0.738
N1	−0.345	−0.306	−1.364	−0.517	−0.475
N2	−0.344	−0.303	−1.364	−0.508	−0.475

values from electron diffraction. The atomic charges on atoms involved in noncovalent interactions within the studied compound are listed in Table 2. Summing of the atomic charges on the atoms of the cation (first four rows) exhibited that the charge of $[SF_3]^+$ is from 0.594 (CM5) to 0.884*e* (NBO). Thus, charge transfer occurs from the ligands to the cation. Nonetheless, the sulfur atom retained its high positive atomic charge of value between 0.718*e* and 2.917*e*. The negative charge on the atoms of the Lewis bases was from −0.305*e* to −1.364*e* for fluorine in the anionic entity and −0.303*e* to −1.364*e* for nitrogen atoms in the acetonitrile ligands. One can notice that the NBO and AIM charges deviate significantly from the others, as illustrated in Fig. 3. The value of NBO is in line with the other methods only for the N1 and N2 atoms, while the AIM approach to charges gives the most extreme results both for positive and negative charges. The method based on electrostatic potential (CHELPG) is closer to the referential CM5 and ADCH ones; however, a certain degree of overvaluation of both positive and negative charges is visible.

The nature of the interactions in the selected fragment of the crystal structure was predicted by the ALMO-EDA scheme. The results are collected in Table 3. According to this protocol, the interaction energy is dissected into electrostatic (ELEC), Pauli repulsion (PAULI), dispersion (DISP), polarization (POL) and charge transfer (CT) components. Additionally, in the penultimate and last columns of Table 3, the interaction

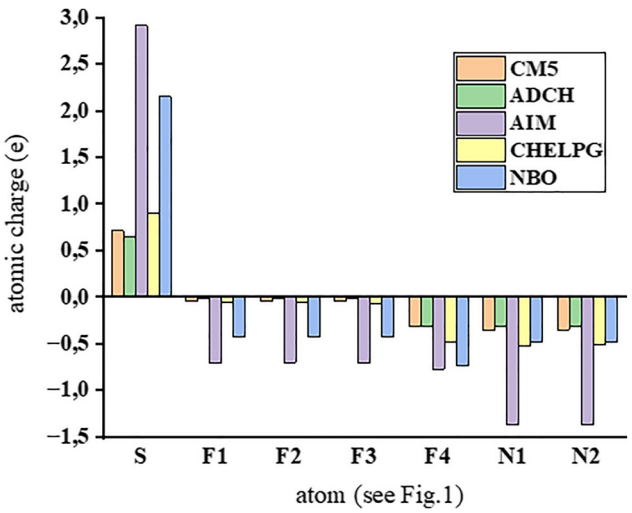

Fig. 3 Atomic charge distribution on selected atoms.

energies are summarized. The M062X/def2tzvpp interaction energies were taken from ALMO-EDA computations in the solvent and corrected for BSSE. All energies concern interactions between the given ligand and the remainder of the studied $[SF_3(NCCH_3)_2][SbF_6]$ system; thus, in each case, two separate units were considered. The M062X interaction energy between the anion and the cation with two neutral ligands attached is −16.66 kcal mol^{-1}, while for the neutral pairs ($[SF_3(NCCH_3)_2][SbF_6]$ *versus* $NCCH_3$) it was worse by around 6 kcal mol^{-1}.

The contribution of individual components of E_{int} in the ALMO-EDA can be explained by pairing them with the CM5 atomic charges. When examining the charges on the atoms directly participating in the cation···anion interaction, namely the sulfur atom from the cation and the F4 atom belonging to the anion, these values are +0.72 and −0.31*e*, respectively (see Table 2). Indeed, the ELEC factor is dominant in this system, accounting for 67% of the total attractive forces, whereas DISP and CT together contribute 26%. The presence of two neutral ligands significantly influences the E_{int}. The charges on the nitrogen atoms of the neutral ligands are even slightly more negative than on F4 and amount to −0.34*e*. These interactions are primarily electrostatic, accounting for 57% of the total attractive components. Compared to the cation···anion interaction, the contribution of the CT term is higher, reaching 19%. The least important term is POL, which was less than 10%.

The QTAIM analysis for the structure highlighted in Fig. 1 confirmed the presence of three bond paths with associated bond critical points (BCPs) between the cation and the ligands (Fig. S1). The electron density (ρ) at BCP can be an indicator of the strength of the examined interactions.[54,58–60] In the current case, these values are 0.028 au and 0.035 au, for the S···F and two S···N interactions, respectively. These values are typical for the noncovalent interactions of intermediate strength. Nonetheless, the ρ values do not reproduce the outcomes of the interaction energies, which signify a distinctly stronger interaction between the ions.

Models with noble gas atoms

The concept of interactions between the sulfonium cation and noble gases assumes that the cation has strong acidic binding sites on the F–S covalent bond extensions, which can attract the highly unreactive Ng atom. However, an interesting question would be whether it is possible to observe such interaction when the cation is partially neutralized by anion or neutral ligands. Therefore, MEP calculations were conducted for two model systems: $[SF_3(NCCH_3)_2]^+$ (cation with two neutral ligands) and $[SF_3][SbF_6]$ (cation with anion). In the former example, the only maximum that occurred at the sulfur atom is 138 kcal mol^{-1}. In the second model, two equivalent maxima of EP are identified on the elongations of the F–S bonds with values equal to 119 kcal mol^{-1}. It should be noted that the maxima for the bare $[SF_3]^+$ cation were around 186–188 kcal.[32] Therefore, a substantial reduction of the electron-accepting power of the sulfonium cation is achieved. A slightly lower value of 104 kcal mol^{-1} was found for the cyclic derivative of the diarylsulfonium cation.[2] Another maximum in the studied system is positioned under the S atom. Its value is 81 kcal mol^{-1}. Although it is still quite intense, the vicinity of the fluorine atoms does not allow the incorporation of a noble gas in this area. A color-coded visualization of the MEP maps is displayed in Fig. 4.

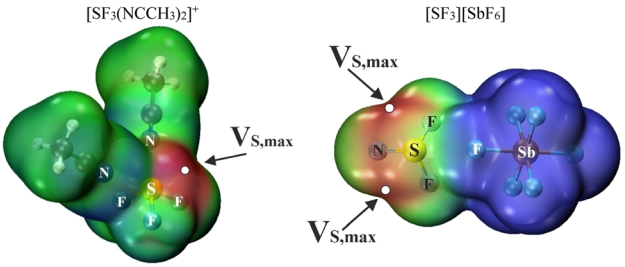

Fig. 4 Molecular electrostatic potentials of two dimers before attaching the Ng atoms. The color scale is arranged from blue (less than +62.7 kcal mol^{-1}) to red (more than +113 kcal mol^{-1}) for the $[SF_3(NCCH_3)_2]^+$ cation and from blue (less than 0 kcal mol^{-1}) to red (more than +100 kcal mol^{-1}) for the $[SF_3][SbF_6]$ system.

The optimized $[SF_3(NCCH_3)_2Ng]^+$ and $[SF_3(Ng)_2][SbF_6]$ complexes are assessed by means of their geometry in Table 4. The general scheme of the discussed tetramers is presented in Fig. 5. In the complexes labelled as **1–3**, the Ng atom was initially put on the coordinates corresponding to the fluorine atom from the $[SbF_6]^-$ anion in the crystal structure, while in complexes **4–6**, two equivalent Ng atoms were placed in the original place of atoms from acetonitriles in the crystal. All six complexes are true minima on the potential energy surface. They exhibit S···Ng distances shorter than the sums of the van der Waals radii of the respective atoms. The length of the S···Ng bond increases with the size of the Ng atom. In general, the incorporation of the Ng atom takes place at a longer distance than the attachment of F or N atoms in the optimized crystal source (compared with Table 1). This lengthening is from 0.9 (complex **5**) to 1.1 Å (complex **3**). This change is accompanied by the simultaneous shortening of the remaining contacts participating in the stabilization of the complexes. The S···N distances are shorter by about 0.01 Å, whereas the S···F ones are by 0.2 Å

Table 3 Contributions of the ALMO-EDA decomposition terms for the $[SF_3(NCCH_3)_2][SbF_6]$ complex. ES = electrostatic term, POL = polarization, CT = charge transfer, DISP = dispersion. Percentage contributions are defined as a fraction of the sum of all attractive components. All data in kcal mol^{-1}

	ELEC	%	PAULI	DISP	%	POL	%	CT	%	E_{int} (M062X)
$[SbF_6]^-\cdots[SF_3(NCCH_3)_2]^+$	−20.99	67	14.57	−4.72	15	−2.09	7	−3.43	11	−16.66
$NCCH_3\cdots[SF_3(NCCH_3)][SbF_6]$	−20.54	57	24.92	−5.26	15	−3.38	9	−6.68	19	−10.94
$NCCH_3\cdots[SF_3(NCCH_3)][SbF_6]$	−20.70	57	25.25	−5.29	15	−3.41	9	−6.81	19	−10.97

Table 4 Geometric parameters of complexes **1–6** (Å and °) as defined in Fig. 4

	R(S···Ng)	R(S···N1)	R(S···N2)	∠F1–S–Ng	∠F2–S–N2	∠F3–S–N1
1	3.553	2.435	2.435	167.0	176.9	176.9
2	3.569	2.433	2.433	164.7	177.1	177.1
3	3.607	2.437	2.437	168.2	177.1	177.1
	R(S···Ng1)	R(S···Ng2)	R(S···F4)	∠F1–S–F4	∠F2–S–Ng2	∠F3–S–Ng1
4	3.553	3.632	2.269	178.5	170.5	178.4
5	3.457	3.467	2.269	178.8	175.4	179.1
6	3.604	3.590	2.276	179.2	163.3	167.3

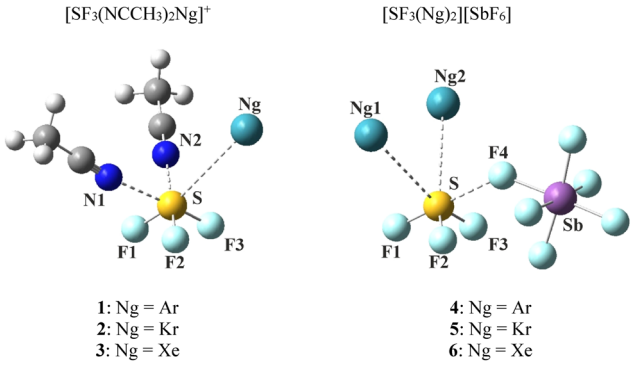

Fig. 5 Molecular diagrams presenting the general scheme of the $[SF_3(NCCH_3)_2Ng]^+$ and $[SF_3(Ng)_2][SbF_6]$ studied complexes.

in comparison with the optimized full $[SF_3(NCCH_3)_2][SbF_6]$ system. Another common trend is that all itemized angles concerning noncovalent interactions in these compounds indicate high proximity to a linear angle. The largest deviation is observed for the F1–S–Ng angle in **2**, which is 164.7°. Therefore, the position of the MEP maxima (which can be termed as σ-holes) at the sulfonium cation is vital for the trajectory of incorporation of the Ng atom. It is important to notice that even when such cations are partially neutralized by an anion or two acetonitrile ligands and immersed in a solvent, they can still bind two neutral, relatively unreactive noble gas atoms.

The atomic charges on selected atoms in complexes **1–6** are shown in Table 5. First, it should be noted that all Ng atoms have positive charges. Their values increase in the order Ar < Kr < Xe, from 0.002*e* to 0.055*e*. This confirms the charge transfer from the Ng atom to the cation. With respect to the sulfur atom, its charge is lessened in relation to the results for the optimized full crystal (see Table 2), except in a few cases. Its growth is observed for complexes **1**, **2**, **4**, **5** and **6** according to the CM5 method and complexes **1–3** by the ADCH and AIM method. Within the set of systems **1–3**, the switching of the $[SbF_6]^-$ anion to a noble gas induces a slight reduction in the charge on the whole cation by a maximum of 0.05*e* (in the CHELPG method). An exception is seen in the CM5 results, which show a marginal rise in this value. Concerning the complexes containing two Ng atoms (**4–6**), the general trend indicates a rise in cation charge across all methods, from 0.02 to 0.18*e*, with the largest increase observed for CHELPG. The intensity of this enlargement can be presented in the order Xe < Kr < Ar. As it was in the case of the charges for the optimized crystal structure, the NBO and AIM approaches show significantly different values of charge, again with the most extreme deviations found for the AIM charges. However, the trends mentioned above are still preserved.

Table 6, similar to Table 3, consolidates the interaction energy terms according to the ALMO-EDA scheme in the solvent medium. For the first three systems in which the $[SbF_6]^-$ anion was replaced by a Ng atom, the interaction energies and their

Table 5 The atomic charges on selected atoms of complexes **1-6**. Numbering of atoms is defined in Fig. 5

Atom	CM5	ADCH	AIM	CHLPG	NBO	Atom	CM5	ADCH	AIM	CHLPG	NBO
	1						**4**				
S	0.725	0.644	2.889	0.873	2.122	**S**	0.783	0.722	2.966	0.810	2.122
F1	−0.023	−0.004	−0.695	−0.018	−0.406	**F1**	−0.017	0.016	−0.682	−0.027	−0.407
F2	−0.044	−0.010	−0.695	−0.067	−0.426	**F2**	0.004	0.022	−0.684	0.017	−0.384
F3	−0.044	−0.010	−0.699	−0.065	−0.426	**F3**	0.005	0.029	−0.682	0.023	−0.384
Ar	0.020	0.021	0.005	0.008	0.003	**F4**	−0.286	−0.301	−0.759	−0.424	−0.740
N1	−0.336	−0.273	−1.367	−0.506	−0.489	**Ar1**	0.024	0.024	0.008	0.022	0.003
N2	−0.336	−0.272	−1.367	−0.513	−0.489	**Ar2**	0.020	0.021	0.006	0.019	0.002
	2						**5**				
S	0.718	0.625	2.883	0.855	2.120	**S**	0.753	0.647	2.949	0.672	2.116
F1	−0.024	0.003	−0.696	−0.013	−0.407	**F1**	−0.021	0.010	−0.688	−0.010	−0.409
F2	−0.045	−0.010	−0.699	−0.065	−0.427	**F2**	0.001	0.039	−0.685	0.042	−0.387
F3	−0.045	−0.010	−0.699	−0.064	−0.427	**F3**	0.001	0.041	−0.684	0.045	−0.386
Kr	0.030	0.032	0.118	0.016	0.006	**F4**	−0.287	−0.305	−0.760	−0.397	−0.739
N1	−0.336	−0.270	−1.367	−0.505	−0.488	**Kr1**	0.043	0.050	0.020	0.049	0.008
N2	−0.336	−0.271	−1.367	−0.509	−0.488	**Kr2**	0.042	0.049	0.019	0.048	0.008
	3						**6**				
S	0.710	0.606	2.875	0.777	2.116	**S**	0.744	0.619	2.931	0.691	2.111
F1	−0.025	0.009	−0.697	0.005	−0.408	**F1**	−0.019	0.019	−0.686	−0.024	−0.409
F2	−0.046	−0.011	−0.699	−0.059	−0.429	**F2**	−0.001	0.039	−0.686	0.039	−0.390
F3	−0.046	−0.011	−0.699	−0.057	−0.428	**F3**	−0.001	0.041	−0.686	0.040	−0.389
Xe	0.043	0.051	0.025	0.055	0.013	**F4**	−0.288	−0.307	−0.761	−0.441	−0.737
N1	−0.336	−0.271	−1.368	−0.487	−0.487	**Xe1**	0.048	0.059	0.030	0.065	0.013
N2	−0.336	−0.272	−1.368	−0.492	−0.487	**Xe2**	0.049	0.060	0.030	0.064	0.013

Table 6 Contributions of the ALMO-EDA decomposition terms for the $[SF_3(NCCH_3)_2Ng]^+$ and $[SF_3(Ng)_2][SbF_6]$ studied complexes (Ng = Ar, Kr, Xe). ES = electrostatic term, POL = polarization, CT = charge transfer, DISP = dispersion. Percentage contributions are defined as fraction of the sum of all attractive components. All data in kcal mol^{-1}

	ES	%	PAULI	DISP	%	POL	%	CT	%	E_{int} (M062X)
Ar···$[SF_3(NCCH_3)_2]^+$	0.13	—	1.05	−0.87	52	−0.12	7	−0.67	41	−0.48
Kr···$[SF_3(NCCH_3)_2]^+$	−0.13	5	1.97	−1.33	50	−0.26	10	−0.95	35	−0.70
Xe···$[SF_3(NCCH_3)_2]^+$	−0.67	13	3.91	−2.19	44	−0.52	10	−1.61	32	−1.08
Ar1···$[SF_3Ar][SbF_6]$	0.43	—	0.72	−0.66	48	−0.14	10	−0.58	42	−0.23
Ar2···$[SF_3Ar][SbF_6]$	0.51	—	0.87	−0.82	48	−0.20	12	−0.69	40	−0.33
Kr1···$[SF_3Kr][SbF_6]$	0.22	—	2.63	−1.52	45	−0.57	17	−1.32	39	−0.57
Kr2···$[SF_3Kr][SbF_6]$	0.21	—	2.72	−1.57	44	−0.60	17	−1.36	39	−0.60
Xe1···$[SF_3Xe][SbF_6]$	−0.33	6	4.30	−2.48	46	−0.75	14	−1.82	34	−1.09
Xe2···$[SF_3Xe][SbF_6]$	−0.25	5	4.04	−2.35	45	−0.75	14	−1.81	35	−1.13

nature noticeably differ from those observed in the case of the $[SF_3(NCCH_3)_2][SbF_6]$ complex (Table 3), which is quite expected as the anionic entity was replaced by a neutral one. The E_{int} values calculated at the M06-2X level range from −0.48 kcal mol^{-1} for Ar···$[SF_3(NCCH_3)_2]^+$ to −1.08 kcal mol^{-1} for Xe···$[SF_3(NCCH_3)_2]^+$. A similar trend is observed when two neutral $NCCH_3$ ligands are replaced by Ng atoms. In these systems (**4–6**), the interaction energies are comparably small, ranging from −0.23 to −1.13 kcal mol^{-1} for Ar···$[SF_3Ar][SbF_6]$ and Xe···$[SF_3Ar][SbF_6]$, respectively. These values are smaller by approximately an order of magnitude than those calculated for the $NCCH_3$···$[SF_3NCCH_3][SbF_6]$ complex (see Table 3).

The ALMO-EDA analysis reveals pronounced differences in both the nature and magnitude of the interaction energy components relative to the initial system without Ng atoms. While the interaction between $[SbF_6]^-$ and $[SF_3(NCCH_3)_2]^+$ was dominated by the electrostatic term, complexes **1** to **3** exhibit a different nature: the ES contribution is only 5–13%, and for the Ar···$[SF_3(NCCH_3)_2]^+$ system it takes even a positive sign. DISP becomes the main component for the Ar···$[SF_3(NCCH_3)_2]^+$, Kr···$[SF_3(NCCH_3)_2]^+$ and Xe···$[SF_3(NCCH_3)_2]^+$ complexes (44–52% of share). Charge transfer, which was a minor contributor in the $[SF_3(NCCH_3)_2]^+$···$[SbF_6]^-$ complex, now accounts for 32–41%. The POL term becomes more important for **3** (10%) compared to **1** (7%), consistent with the higher polarizability of Xe than Ar. This situation is repeated in the noble gas complexes **4–6**, where the ES contribution is marginal and, in four cases, is repulsive. For these complexes, the mix of DISP and CT is responsible for most of the attractive forces (80 to 90%). It must be emphasized that the interaction energies around −1 kcal mol^{-1} fall into the lower limit of the range detected for noble gas···halonium cation systems studied earlier, where they were around −1 kcal mol^{-1} for the complexes between $[C_3H_6I]^+$ and Ar.[31]

The Bader's QTAIM analysis shows bond paths between sulfur and noble gas atoms for every studied complex (Fig. S2). However, the ρ values range from 0.005 to 0.009 au, which validates that these interactions are very weak and, in fact, close to the limit of detection by this method. At the same time, the remaining interactions in the models increase in strength, as the ρ values for the S···N and S···F contacts are larger by 0.008 to 0.018 au than in the $[SF_3(NCCH_3)_2][SbF_6]$ complex.

Conclusion

In the current work, the limits of the electrophilic abilities of the chalconium cations were tested. The weakest one of these species (the sulfonium cation) was studied in a series of complexes with inert noble gases, which are known for their poor reactivity. Additionally, the potential of its acidic binding sites was weakened by immersing it in the dichloromethane medium (mimicked by the PCM solvent model) and partial neutralization by the anionic and neutral ligands that were present in the crystal structure. The six tetramers, namely three $[SF_3(NCCH_3)_2Ng]^+$ and three $[SF_3(Ng)_2][SbF_6]$ (Ng = Ar, Kr, Xe) ones, were successfully optimized, although their interaction energies oscillate around −1 kcal mol^{-1}. Replacing the $[SbF_6]^-$ anion with a noble gas atom results in a significant weakening of the interaction energy of such systems and a change in their nature from electrostatic (which was expected for interactions between oppositely charged ions as in the crystal structure) to one controlled by comparable contributions of the DISP and CT terms, with a slight predominance of the former. The tendency for the absolute value of E_{int} to increase in the Ar < Kr < Xe series reflects the growing role of POL, which is consistent with the increase in atomic radius and polarizability of Ng atoms in this order. The situation is analogous in the case of replacing $NCCH_3$ ligands with two noble gas atoms. E_{int} becomes significantly smaller, and its character gets directed mainly by the CT term. The performed theoretical analyses for the model constructs indicate that the binding of noble gas atoms by the sulfonium cation is possible, although modest; yet their integration into the cation boosts the strength of the S···N or S···F noncovalent interactions residing in the analyzed systems.

Conflicts of interest

There are no conflicts to declare.

Data availability

The data supporting this article has been included as part of the supplementary information (SI). Supplementary information is available. See DOI: https://doi.org/10.1039/d5cp04672f.

Acknowledgements

The authors (M.M. and W.Z.) gratefully acknowledge Wrocław Center for Networking and Supercomputing (WCSS). This work was financed *via* the grant ''MINIATURA'' from the National Science Centre (Poland) awarded to M.M, with grant number 2025/09/X/ST4/00174.

References

1 L. Groslambert, A. Padilla-Hernandez, R. Weiss, P. Pale and V. Mamane, *Chem. – Eur. J.*, 2023, **29**, e202203372.
2 A. S. Novikov and D. S. Bolotin, *Org. Biomol. Chem.*, 2022, **20**, 7632–7639.
3 I. O. Putnin, A. A. Sysoeva, A. V. Kovalenko and D. S. Bolotin, *Org. Biomol. Chem.*, 2025, **23**, 7197–7205.
4 A. A. Sysoeva, Y. V. Safinskaya, M. V. Il'in, A. S. Novikov and D. S. Bolotin, *Org. Biomol. Chem.*, 2025, **23**, 1970–1980.
5 K. Bläsing, R. Labbow, D. Michalik, F. Reiss, A. Schulz, A. Villinger and S. Walker, *Chem. – Eur. J.*, 2020, **26**, 1640–1652.
6 X. He, X. Wang, Y.-L. Tse, Z. Ke and Y.-Y. Yeung, *Angew. Chem., Int. Ed.*, 2018, **57**, 12869–12873.
7 R. Weiss, E. Aubert, P. Pale and V. Mamane, *Angew. Chem., Int. Ed.*, 2021, **60**, 19281–19286.
8 B. Y. Zhou and F. P. Gabbaï, *J. Am. Chem. Soc.*, 2021, **143**, 8625–8630.
9 M. V. Il'in, A. S. Novikov and D. S. Bolotin, *J. Org. Chem.*, 2022, **87**, 10199–10207.
10 Y. Lu, Q. Liu, Z. X. Wang and X. Y. Chen, *Angew. Chem., Int. Ed.*, 2022, **61**, e202116071.
11 A. A. Kuznetsova, V. V. Yanshole, M. V. Il'in, A. S. Novikov, D. S. Bolotin, M. N. Sokolov and P. A. Abramov, *Inorg. Chem. Front.*, 2024, **11**, 8902–8915.
12 A. Dhaka, O. Jeannin, E. Aubert, E. Espinosa and M. Fourmigué, *Chem. Commun.*, 2021, **57**, 4560–4563.
13 A. A. Ganie, A. A. Ahangar and A. A. Dar, *Cryst. Growth Des.*, 2019, **19**, 4650–4660.
14 G. Resnati, P. Scilabra and G. Terraneo, *Acta Crystallogr., Sect. A*, 2019, **75**, E488–E488.
15 P. Scilabra, G. Terraneo and G. Resnati, *Acc. Chem. Res.*, 2019, **52**, 1313–1324.
16 G. K. H. Shimizu, R. Vaidhyanathan and J. M. Taylor, *Chem. Soc. Rev.*, 2009, **38**, 1430–1449.
17 C. B. Aakeroy, D. L. Bryce, G. Desiraju, A. Frontera, A. C. Legon, F. Nicotra, K. Rissanen, S. Scheiner, G. Terraneo, P. Metrangolo and G. Resnati, *Pure Appl. Chem.*, 2019, **91**, 1889–1892.
18 S. Benz, J. López-Andarias, J. Mareda, N. Sakai and S. Matile, *Angew. Chem., Int. Ed.*, 2017, **56**, 812–815.
19 P. Politzer, J. S. Murray, T. Clark and G. Resnati, *Phys. Chem. Chem. Phys.*, 2017, **19**, 32166–32178.
20 J. S. Murray, P. Lane, T. Clark, K. E. Riley and P. Politzer, *J. Mol. Model.*, 2012, **18**, 541–548.
21 J. S. Murray, P. Lane, T. Clark and P. Politzer, *J. Mol. Model.*, 2007, **13**, 1033–1038.
22 A. Bauza and A. Frontera, *Phys. Chem. Chem. Phys.*, 2015, **17**, 24748–24753.
23 A. Bauza and A. Frontera, *Angew. Chem., Int. Ed.*, 2015, **54**, 7340–7343.
24 M. D. Esrafili, F. Mohammadian-Sabet and M. Solimannejad, *Chem. Phys. Lett.*, 2016, **659**, 196–202.
25 M. D. Esrafili and F. Mohammadian-Sabet, *Chem. Phys. Lett.*, 2017, **667**, 337–344.
26 W. Zierkiewicz, M. Michalczyk and S. Scheiner, *Phys. Chem. Chem. Phys.*, 2018, **20**, 4676–4687.
27 R. Wang, H. Liu, Q. Li and S. Scheiner, *Phys. Chem. Chem. Phys.*, 2020, **22**, 4115–4121.
28 R. J. Wang, Z. Wang, X. F. Yu and Q. Z. Li, *ChemPhysChem*, 2020, **21**, 2426–2431.
29 S. Borocci, F. Grandinetti and N. Sanna, *Chem. Phys. Lett.*, 2023, **819**, 140443.
30 R. Pino-Rios, A. Vasquez-Espinal, S. Pan, E. Cerpa, W. Tiznado and G. Merino, *ChemPhysChem*, 2023, **24**, e202200601.
31 W. Zierkiewicz, S. Scheiner and M. Michalczyk, *Phys. Chem. Chem. Phys.*, 2024, **26**, 25762–25766.
32 D. Turnbull, P. Chaudhary, P. Hazendonk, S. D. Wetmore and M. Gerken, *Inorg. Chem.*, 2021, **60**, 3893–3901.
33 C. R. Groom, I. J. Bruno, M. P. Lightfoot and S. C. Ward, *Acta Crystallogr., Sect. B*, 2016, **72**, 171–179.
34 F. Weigend, *Phys. Chem. Chem. Phys.*, 2006, **8**, 1057–1065.
35 F. Weigend and R. Ahlrichs, *Phys. Chem. Chem. Phys.*, 2005, **7**, 3297–3305.
36 Y. Zhao and D. G. Truhlar, *Acc. Chem. Res.*, 2008, **41**, 157–167.
37 Y. Zhao and D. G. Truhlar, *Theor. Chem. Acc.*, 2008, **120**, 215–241.
38 M. J. Frisch, G. W. Trucks, H. B. Schlegel, G. E. Scuseria, M. A. Robb, J. R. Cheeseman, G. Scalmani, V. Barone, G. A. Petersson, H. Nakatsuji, X. Li, M. Caricato, A. V. Marenich, J. Bloino, B. G. Janesko, R. Gomperts, B. Mennucci, H. P. Hratchian, J. V. Ortiz, A. F. Izmaylov, J. L. Sonnenberg, F. Williams, F. Ding, F. Lipparini, F. Egidi, J. Goings, B. Peng, A. Petrone, T. Henderson, D. Ranasinghe, V. G. Zakrzewski, J. Gao, N. Rega, G. Zheng, W. Liang, M. Hada, M. Ehara, K. Toyota, R. Fukuda, J. Hasegawa, M. Ishida, T. Nakajima, Y. Honda, O. Kitao, H. Nakai, T. Vreven, K. Throssell, J. A. Montgomery Jr., J. E. Peralta, F. Ogliaro, M. J. Bearpark, J. J. Heyd, E. N. Brothers, K. N. Kudin, V. N. Staroverov, T. A. Keith, R. Kobayashi, J. Normand, K. Raghavachari, A. P. Rendell, J. C. Burant, S. S. Iyengar, J. Tomasi, M. Cossi, J. M. Millam, M. Klene, C. Adamo, R. Cammi, J. W. Ochterski, R. L. Martin, K. Morokuma, O. Farkas, J. B. Foresman and D. J. Fox, *Gaussian 16*, Wallingford, CT, 2016.
39 A. Bauza, I. Alkorta, A. Frontera and J. Elguero, *J. Chem. Theory Comput.*, 2013, **9**, 5201–5210.
40 S. Kozuch and J. M. L. Martin, *J. Chem. Theory Comput.*, 2013, **9**, 1918–1931.
41 R. Cammi, B. Mennucci and J. Tomasi, *J. Phys. Chem. A*, 2000, **104**, 4690–4698.
42 J. Tomasi, B. Mennucci and R. Cammi, *Chem. Rev.*, 2005, **105**, 2999–3093.
43 T. Lu and F. Chen, *J. Mol. Graphics Modell.*, 2012, **38**, 314–323.

44 T. Lu and F. Chen, *J. Comput. Chem.*, 2012, **33**, 580–592.
45 W. Humphrey, A. Dalke and K. Schulten, *J. Mol. Graphics Modell.*, 1996, **14**, 33–38.
46 P. R. Horn, Y. Mao and M. Head-Gordon, *Phys. Chem. Chem. Phys.*, 2016, **18**, 23067–23079.
47 P. R. Horn, Y. Mao and M. Head-Gordon, *J. Chem. Phys.*, 2016, **144**, 114107.
48 S. F. Boys and F. Bernardi, *Mol. Phys.*, 1970, **19**, 553–566.
49 A. V. Marenich, S. V. Jerome, C. J. Cramer and D. G. Truhlar, *J. Chem. Theory Comput.*, 2012, **8**, 527–541.
50 T. Lu and F. Chen, *J. Theor. Comput. Chem.*, 2012, **11**, 163–183.
51 P. Bultinck, R. Vanholme, P. L. A. Popelier, F. De Proft and P. Geerlings, *J. Phys. Chem. A*, 2004, **108**, 10359–10366.
52 C. M. Breneman and K. B. Wiberg, *J. Comput. Chem.*, 1990, **11**, 361–373.
53 F. Weinhold, C. R. Landis and E. D. Glendening, *Int. Rev. Phys. Chem.*, 2016, **35**, 399–440.
54 R. Bader, *Atoms In Molecules. A Quantum Theory*, Clarendon Press, Oxford, 1990.
55 R. F. W. Bader, *J. Phys. Chem. A*, 1998, **102**, 7314–7323.
56 T. A. Keith and T. K. Gristmill, Software: Overland Park KS, 2013.
57 S. Mahmoudi, T. Gruene, C. Schroder, K. D. Ferjaoui, E. Frojdh, A. Mozzanica, K. Takaba, A. Volkov, J. Maisriml, V. Paunovic, J. A. van Bokhoven and B. K. Keppler, *Nature*, 2025, **645**, 88–94.
58 S. J. Grabowski, *J. Phys. Chem. A*, 2012, **116**, 1838–1845.
59 R. F. W. Bader and H. Essen, *J. Chem. Phys.*, 1984, **80**, 1943–1960.
60 P. S. V. Kumar, V. Raghavendra and V. Subramanian, *J. Chem. Sci.*, 2016, **128**, 1527–1536.

